JOURNAL OF APPLIED PHYSICS **101**, 124303 (2007)

Nanospot welding and contact evolution during cycling of a model microswitch

Christopher M. Doelling and T. Kyle Vanderlick[a]
Department of Chemical Engineering, Princeton University, Princeton, New Jersey 08544

Jun Song
Department of Mechanical and Aerospace Engineering, Princeton University, Princeton, New Jersey 08544

David Srolovitz
Yeshiva College, Yeshiva University, New York, New York 10033

(Received 7 March 2007; accepted 30 April 2007; published online 18 June 2007)

The useful lifetime of microelectromechanical system switches is shortened during repetitive contact when the continual making and breaking of an electrical circuit accelerates damage done to the metallic contact points in the switch. In this study the interfacial force microscope is used as a model switch, and we explore the fundamental processes involved in switch failure. We find that repeated indentation (cyclic contact) causes protective coatings (in the form of self-assembled monolayers) to fail allowing metal-metal intimacy and formation of a malleable "nanospot weld." The weld is stretched during separation of the contacting surfaces, leading to the development of nanoasperities. With the help of atomistic simulations, which provide insight into material transfer and consequential roughening of the surfaces, we show that asperity length grows with continued repetition, drastically changing the resistance of the contact over the lifetime of the switch. Controlling the amount of current passed through the contact influences the extent of weld stretching and arcing observed during contact separation. © *2007 American Institute of Physics*
. [DOI: 10.1063/1.2747229]

I. INTRODUCTION

Microswitches are becoming increasingly present in modern electronic devices. Their small size, light weight, low cost, and superior signal quality (exceeding that of presently used solid state devices[1,2]) make them particularly appealing for use in the portable electronics industry. Unfortunately, their performance is unreliable due to failure. In particular, the useful lifetime of microswitches is shortened during repetitive contact, wherein the continual making and breaking of an electrical circuit accelerates damage done to the metallic contact points in the switch. The two primary modes of failure in these devices are the permanent sticking of the two contacts and the catastrophic or continual rise in contact resistance above a specified value. Inconsistent resistance behavior further manifests itself early in the switch's cycling lifetime, where contact resistance is found to decrease with cycling, a trend opposite to that found in later cycles.[3] Unreliable and inconsistent performance is the main issue limiting the commercial application of microelectromechanical system (MEMS) switches to a larger market.

A typical MEMS switch consists of a cantilever suspended above a stationary metal electrode. At the end of the cantilever arm is a metallic tip, which when brought into contact with the electrode completes the circuit. The cantilever arm must be bent (actuated) for this to occur, and in turn must also act as the restoring force used to separate the electrodes. Minimizing the force required to make and break a valid contact will not only consume less power, but also make the switch faster and lighter. Stronger adhesion between contact points necessitates stiffer cantilevers and thus larger forces. Large actuation forces may also be required to create low resistance contacts (e.g., to break through contamination). Oftentimes, these two design problems are coupled; for example, using alloys which minimize adhesion between contacts comes at the cost of increased resistance.[4] Therefore, maximizing switch efficiency requires minimizing both the adhesion and the amount of force necessary to make a low resistance contact.

Surface modification strategies such as self-assembled monolayers (SAMs) provide a convenient means to deliver the right balance between antiadhesive and electrical characteristics. Additionally, several species of SAMs, most notably those containing conjugated bonds, have demonstrated conduction property characteristics of resistors and wires.[5] Ideally, the SAM layers will absorb impact energy, protecting the surface from damage, and envelope the contact point in a repeatable, low resistance area. From a more practical standpoint, the deliberate application of a molecular coating provides a means to tune surface properties that are otherwise controlled by unavoidable contamination. When exposed to air, for example, a hydrocarbon contamination layer will spontaneously adsorb on gold, a common electrode material. While these unwanted hydrocarbons minimize adhesion, they adversely affect the contact's conductive properties. In a recent study by Tringe *et al.*,[6] the presence of a contamination layer was blamed for the lack of consistent contact events, regardless of the forces used.

Fundamental studies of switches and electrical contact

[a]Author to whom correspondence should be addressed; electronic mail: vandertk@princeton.edu

0021-8979/2007/101(12)/124303/7/$23.00 © 2007 American Institute of Physics

Downloaded 28 Jun 2007 to 128.112.35.157. Redistribution subject to AIP license or copyright, see http://jap.aip.org/jap/copyright.jsp

phenomena have centered on contact resistance measurements as summarized in the 1950s by Holms in his classic text, *Electrical Contacts Handbook*.[7] More recent summaries also exist (e.g., Slade[8]). Early experiments were limited by technology and focused on large scale devices (e.g., breaker switches) under conditions of high forces and currents. Today, MEMS-level experiments using the devices themselves,[9,10] or nanoindentation platforms,[11–14] dominate the landscape. Recent studies, using normal switch operating voltages and forces, show the complex evolution of contact resistance over switch lifetime,[3,9,15] localized melting phenomena,[11,12,16] and also the influence of contaminants on the integrity of the contact.[6,13] As with real MEMS switches, the contacting surfaces are generally used multiasperity. While computational modeling of these complicated contacts has been helpful in interpreting the resistance data,[17–20] they limit discussion of the fundamental processes which happen at individual asperities.

In this work we use the interfacial force microscope (IFM) to create a prototypical MEMS switch and follow contact evolution as a result of repeated cycling. The IFM provides a well defined geometry in the form of an electrochemically smooth parabolic tip (of microns in size) interacting with an atomically flat surface that can be modified with a protective SAM coating. The unique force management capabilities of the IFM allow the stable approach and withdrawal of the two contacts and simplifies the mechanical analysis. Moreover, through use of minimal currents and voltages, we can focus on the fundamental processes present in this model MEMS contact. One such process is asperity evolution during switch operation (i.e., repeated contact). We study this not only experimentally but also through atomistic simulations of a flat immobile surface brought repeatedly into contact with a single gold asperity.

While the primary focus of this investigation is the role of repetitive cycling on the evolution of surface topography and resistance in a model switch contact, a secondary objective is to study the behavior of SAM coatings when subjected to cyclic loading events. Notably, while these molecular coatings appear robust in one-time compressions,[21,22] their performance under conditions of repetitive contact is not well characterized.

Although SAMs have proven to remain intact in nanoindentation, they have also been shown to displace at a critical pressure,[23] which is the key operating principle behind techniques such as nanografting,[24] dip-pen nanolithography,[25] and nanopen reader and writer (NPRW).[26] We find that repetitive contact, not necessarily the exceeding of a critical force, degrades the monolayers to the point where prevention of a localized penetration is no longer guaranteed. In this work we find that localized penetration of the monolayer (conditions are SAM specific) initiates changes in topography, which may lead to eventual failure of the device.

II. METHODS

The interfacial force microscope (IFM) is a unique scanning probe technique developed at Sandia National Laboratories and more thoroughly described in existing literature.[27] The key feature of this instrument is its ability to maintain sensor stability, avoiding snap-to and pull-off mechanical instabilities. A force feedback controller prevents the cantilever instability seen in other scanning probe methods, such as the atomic force microscope (AFM), and as a result, quantitative data is collected throughout the entire range of the force-displacement curve without damaging the surfaces due to impact of the contact points. This lack of impact allows contact evolution to be observed in fewer cycles because the topography changes initiated in the previous cycles are carried forward to the next. Experiments were conducted at constant velocity (9.4 Å/s) to better allow full development of changes in contact topography. Force-displacement data is processed such that zero relative displacement corresponds to the maximum or turn-around force and positive displacements reflect the distance relative to this point.

Gold probe tips are electrochemically etched from 0.5 μm diameter 99.99% pure gold wire, and are smooth and parabolic. Their parabolic shape and radius of curvature are characterized by imaging on an FEI/hillips XL 30 field emission gun scanning electron microscope (FEG-SEM). The typical radius of curvature is $\sim$2.5 μm. The tips are dipped in piranha solution, rinsed in pure water, and cleaned with an ultraviolet ozone cleaning system prior to use.

Electrical contact resistance measurements are collected simultaneously with force measurements utilizing a constant current power supply (CCPS). In our measurements, current is maintained at one of two preset values, and we monitor changes in voltage as the contact resistance changes. The low current setting is 50 nA, and the high current setting is 1000 nA. To prevent overloading the circuit when the tip and surface are out of contact ($R_c=\infty$), voltage is limited to a maximum of $\sim$2.7 V.

Hexadecanethiol, hexanethiol, and benzenemethanethiol (BMT) molecules were obtained from Sigma-Aldrich. The monolayers were formed from relatively dilute (100 μM) ethanolic solutions on the (111)-oriented facets of single crystal gold (atomically flat single crystal gold surfaces form naturally during the flame annealing of 99.99% pure gold wire). Past experience has shown that long exposures (48 h) in dilute thiol solutions produces high-quality films.[28] Experiments are conducted in a dry (<5% humidity) nitrogen environment at room temperature and pressure.

We performed a series of molecular dynamics (MD) simulations of asperity contact under cyclic loading in a system containing $\sim 10^4$ gold atoms, as described using the embedded atom method[29,30] (EAM) potential for gold developed by Cai and Ye.[31] This potential offers reasonable descriptions of both bulk and surface phenomena. The simulations focused on a single asperity on a thick substrate that is repeatedly brought into contact with and separated from a rigid flat. The atomic configuration of the initial asperity was formed by placing a small cube of gold atoms on the substrate and relaxing it through a series of thermal treatments.[32] The asperity initially contained 1280 atoms and had a radius of $\sim$2.5 nm. The simulation cell is periodic along the [100] and [010] directions. The simulation cell size in these directions adjusts freely during the simulations in order to keep the normal stresses zero so as to minimize the mechanical

Downloaded 28 Jun 2007 to 128.112.35.157. Redistribution subject to AIP license or copyright, see http://jap.aip.org/jap/copyright.jsp

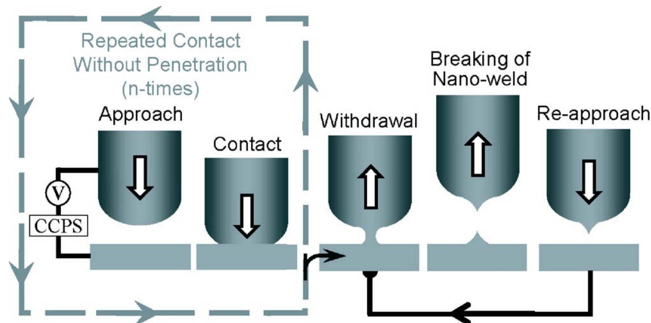

FIG. 1. (Color online) Schematic illustrating the generalized process which occurs when a gold tip is repeatedly brought into contact with a gold surface protected by a self-assembling monolayer. Nonmetallic contact can be repeated several times, until monolayer failure triggers the formation of a metallic nanospot weld, which roughens the surfaces as the weld is ruptured during withdrawal.

coupling between the asperity and its periodic images. The simulations were performed at 300 K. The rigid flat was brought toward (away from) the substrate at a constant velocity of 1 m/s (−1 m/s) along the [001] direction. Hence, these simulations correspond to displacement-controlled, rather than load-controlled, experiments. The direction of the loading was reversed once the rigid flat was within 0.7 nm of the nominal substrate (recall that the initial, hemispherical asperity radius was ~2.5 nm). When the system is unloaded, the rigid flat was retracted to a distance such that the two surfaces were no longer in contact.

III. RESULTS AND DISCUSSION

In this work we use the IFM to create a model MEMS switch and investigate the consequences of repetitive contact, both on the evolution of contact resistance and surface topography, as well as the behavior of SAM coatings. The basic experiment involves the repeated contact (up to a maximum force) and withdrawal of a large ($R\sim2.5$ μm), initially smooth gold tip with a SAM-coated gold surface. Although SAM coatings are robust enough to prevent metal-metal adhesion in a single contact situation (even when taken to relatively high forces, such as that used in nanoindentation[21,22]), one of our key findings is that repeated indentation (cyclic contact) causes these protective coatings to fail, allowing metal-metal intimacy in the form of a malleable "nanospot weld." Moreover, the stretching and rupture of this metal junction creates a nanoasperity whose evolution can be systematically studied.

To best understand the process and associated phenomena, we start with a generalized schematic. As shown in Fig. 1, contact between the tip and SAM-coated substrate occurs n times (n being SAM specific and discussed later) without penetration of the protective layer. On the very next approach (cycle $n+1$), the protective organic layer is displaced resulting in a localized, nanoscopic, breakthrough event as revealed by electrical contact resistance (ECR) measurements. Current flow through the point of contact causes localized heating and the formation of a spot weld. The weld stretches as the tip is retracted, eventually breaking, resulting in a spikelike extremity on a previously smooth surface. This

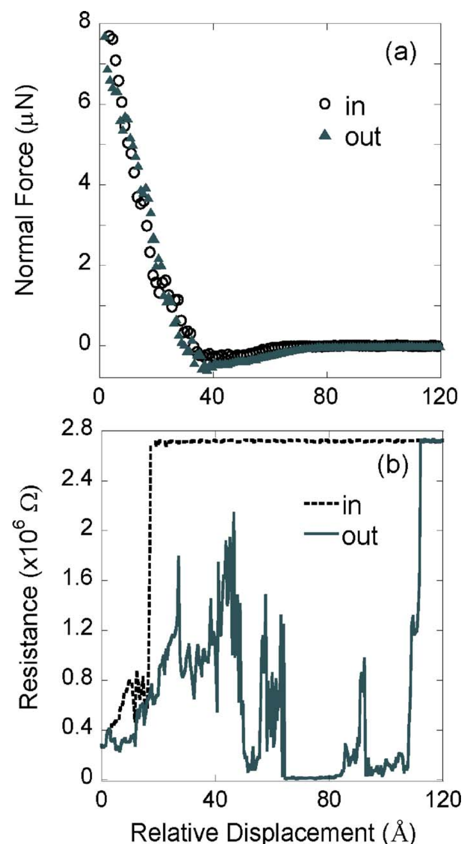

FIG. 2. (Color online) (a) Force profile (force vs displacement) and (b) electrical contact resistance profile (resistance vs displacement) for the "breakthrough" cycle of a gold tip interacting with a gold surface and a hexanethiol monolayer. Shown are both the approach and withdrawal portions of the cycle. Failure of the hexanethiol monolayer (breakthrough) is signaled by the sudden drop in resistance at a repulsive force of approximately 3 μN, followed by a notably chaotic resistance profile during withdrawal with electrical contact present beyond detectable mechanical measurements.

sharp nanoprojection permits electrical contact earlier in reapproach cycle $n+2$, or, if the tip is taken to a previously untouched location, the breakthrough occurs easily (at low force) and at initial contact. Evolution of this nanoasperity can be tracked upon further cycling, leading to an overall roughening of the surfaces and observable changes in the contact's resistance behavior.

A specific example of this process is illustrated in Fig. 2 for the case of a hexanethiol monolayer loaded repeatedly to an arbitrary maximum force of 8 μN. Here the moment of breakthrough, occurring after ten cycles and at a force substantially lower than the maximum, is signaled by a sharp drop in measured resistance, indicating localized disruption of the monolayer. What is not shown are the previous ten profiles where, in spite of the force being repeatedly taken above the resultant breakthrough force, the measured resistance remained at its maximum.

Simple Hertzian-type mechanical analysis shows that at a force of 8 μN, we develop a pressure under the tip of ~0.2 GPa, which is well below the "critical pressure" observed by Xiao *et al.*[23] (0.8 GPa). This demonstrates that a localized penetration event is not dependent upon exceeding a critical pressure, but is more dependent upon how

Downloaded 28 Jun 2007 to 128.112.35.157. Redistribution subject to AIP license or copyright, see http://jap.aip.org/jap/copyright.jsp

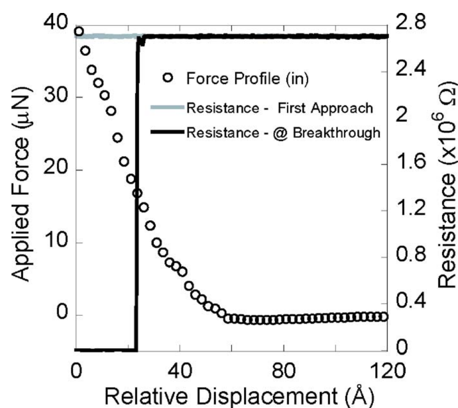

FIG. 3. (Color online) Electrical contact resistance profiles (resistance vs displacement) for both the before and the breakthrough cycle of a gold tip interacting with a gold surface and a hexanethiol monolayer. Shown is the approach portion of the cycle, taken to a maximum force of 40 μN. Early profiles (e.g., the "before" cycle) of this series show resistance remaining at its maximum—the monolayer remains intact. Failure of the hexanethiol monolayer (breakthrough) is signaled by the sudden drop in resistance at a repulsive force of approximately 15 μN.

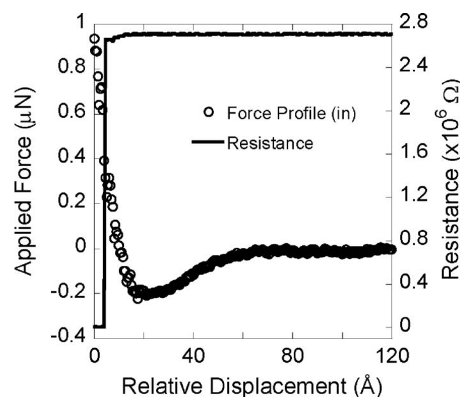

FIG. 4. (Color online) Force and electrical contact resistance profiles of a reapproach (after-breakthrough) cycle, at a different location (an undamaged section of the hexanthiol film used for Fig. 3). Shown are the approach portions of the cycle only. The existence of an asperity is demonstrated by penetrating at a significantly lower force.

damaged/disorganized the film is due to repetition. As might be intuitively expected, if the process involves use of higher maximum force, the breakthrough occurs at fewer repetitions. For example, as shown in Fig. 3, when subjected to a maximum force of 40 μN (creating a pressure under the tip closer to the reported critical pressure), the breakthrough occurs at the third approach as revealed by the sharp drop in resistance.

One expects conditions for monolayer breakthrough to depend on the molecular features of the films, especially the degree of molecular order. While not the explicit focus of this current work, it is useful to provide a few examples to demonstrate this trend. Three different monolayers are compared. One is a 16 carbon alkanethiol, an electrically insulative coating that consistently produces a densely packed monolayer with few defects. Hexanethiol, mentioned previously, is similarly considered as a high resistance coating, although generally not as well organized as the longer thiol. Finally, BMT has a similar molecular height as hexanethiol (6+1 Å), but has a molecular structure which prevents efficient packing. Hexadecanethiol films are the most difficult to penetrate—requiring the most cycles at a given maximum force. Meanwhile, BMT allows easy penetration, occurring almost immediately, at low force and within a few cycles. Lastly, we note that one can effectively modulate SAM order for a given monolayer by varying thiol concentration in the film-forming solution (with higher concentrations yielding more disordered films). Using this approach to affect film order, we further confirm that the more organized the film the more robust it is to repeated contact.

As MEMS devices often have coatings on both surfaces, we also briefly explored the parallel situation in our model switch, where both tip and substrate were coated with SAMs. These experiments are difficult, in practice, because prolonged exposure of the IFM sensor to the ethanolic SAM-forming solution degrades the sensor response and sensitivity. Nevertheless, we managed to perform a few "double-sided SAM" experiments, and these follow the trends discussed above. (Data for BMT coated surfaces are, for example, included in Fig. 9)

Regardless of the specific conditions required for breakthrough, once it occurs, the switch behavior is driven by the development and evolution of a stretchable metallic link between the tip and substrate (a nanospot weld). Its formation is signaled by a drop in resistance on approach, and its behavior as the model switch is opened (i.e., as the tip and substrate are separated) is also revealed through electrical measurements. During withdrawal, as shown in Fig. 2, electrical contact is seen extending well beyond the point of detectable mechanical contact. Here we see the advantage of using electrical measurements to monitor the stretching of the small metallic bridge that is too small to influence the overall mechanical behavior of the system. Use of the IFM is critical to the drawing of the nanoweld because it allows us to retract the tip from the substrate continuously with no mechanical instability (i.e., no jump out). As seen in Fig. 2, at approximately 5 nm this bridge breaks, leaving behind a spikelike extension. Sudden and chaotic jumps seen in the resistance profile beyond 5 nm are attributed to arcing[7,33] (discussed further below). Figure 4 demonstrates the existence of the asperity by performing a reapproach cycle at a different location (an undamaged section of the film) and penetrating at significantly lower forces.

As discussed previously, the evolution of this nanoasperity can be followed as a function of further cycling and can be linked both to fundamental studies of asperity development,[34] as well as contact resistance behavior seen in actual devices. In short we find that, once formed, the substrates make electrical contact sooner and sooner in reapproach cycles, additionally correlating to a systematic decrease in the minimum attractive force, as shown in Fig. 5. Also of notable interest is that the resistance profile of the approach cycles has drastically changed over the course of a relatively small number of cycles. In particular, the later approach cycles are distinctly less sharp and reflect some change in the "landscape" of the contact.

To understand asperity evolution during repeated contact we turn to atomistic simulations for further insight. Con-

Downloaded 28 Jun 2007 to 128.112.35.157. Redistribution subject to AIP license or copyright, see http://jap.aip.org/jap/copyright.jsp

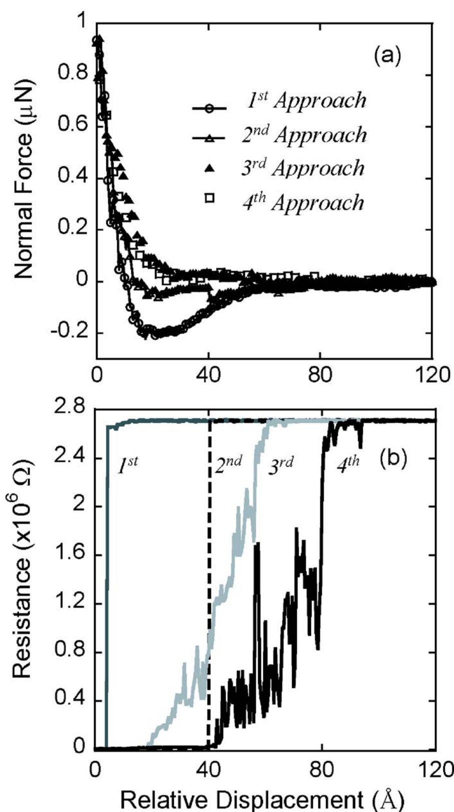

FIG. 5. (Color online) Repeated approach series (approach profile data only) illustrating the continued growth of an asperity as cycles progress. Growth is signaled by an (b) early and earlier point of electrical contact and (a) a decrease in the maximum attractive force due to steric compression of the asperity.

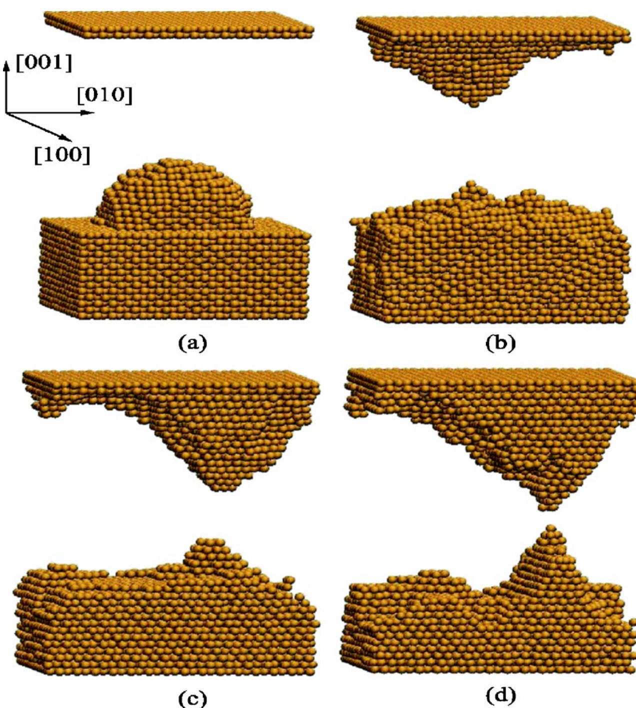

FIG. 6. (Color online) Configuration of the atomistic simulation model of repeated asperity/rigid surface contact. (a) The initial configuration before contact. The configuration of the system after the system was unloaded following the (b) fourth, (c). eighth, and (d) tenth contact.

straints on processing time limit our simulations to phenomenon occurring at the nanoscale ($\sim 10^4$ gold atoms); however, since the postbreakthrough cycles develop asperities having nanoscopic dimensions, comparison between simulation and experiment is appropriate. While a complete analysis of the simulations will be reported in the future, key features related to this study are presented here. Figure 6 shows still frame images from the atomistic simulations of an initially flat (immobile) gold contact being brought, repeatedly, into compression with a single gold asperity. The evolution of contact is dramatic, characterized by a large amount of material transfer and increased texturing of both surfaces. The net effect is, essentially, a roughening of the contacts which gives rise to earlier and earlier electrical conduction during cycling, as shown in Fig. 7. As the simulations do not electrify the contact, the onset of conduction is related to the development of an area of intimate contact. The simulation results are strikingly similar to the experimental results (see Fig. 5).

The growth of surface roughness can be observed by tracking the relative change in displacement, from one approach cycle to the next, corresponding to the onset of conduction. These changes reflect an increase in the effective maximum asperity length, which is how we cast the data. This is shown in Fig. 8 for the simulation. A similar plot, Fig. 9, is shown for experimental results for a variety of contacts (i.e., different SAM-coated substrates). Clearly the trend is upward (contact made sooner, requiring less displacement) although the stochastic nature of the material transfer and atomic rearrangements causes fluctuations in the asperity length (or lengths as the case may be, since multiple asperities are seen to form in the simulations). Since MEMS contacting surfaces start out rough at the nanoscale, we expect contact evolution to follow the same basic trends reported; however, the operating variables (velocity of approach, forces at impact, currents, and voltages) are expected to change the dynamics of the process.

The increasing roughness also has an effect on the experimentally observed forces. The interactions between the

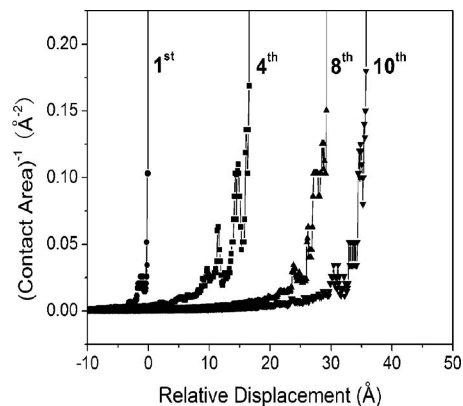

FIG. 7. (Color online) The inverse contact area (proportional to contact resistance) vs relative displacement of the two surfaces in the atomistic simulations. Comparison of the simulation results and the experimental observations (Fig. 5) show an excellent correspondence—sharp jumps that move toward larger displacement with repeated contact. Zero relative displacement corresponds to the displacement at which the two surfaces separate on unloading during the earliest cycle.

Downloaded 28 Jun 2007 to 128.112.35.157. Redistribution subject to AIP license or copyright, see http://jap.aip.org/jap/copyright.jsp

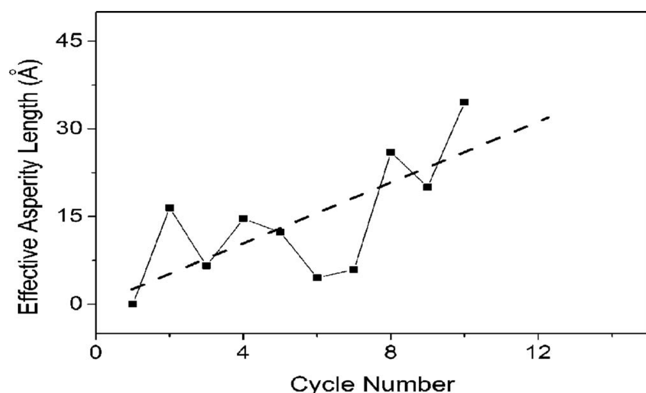

FIG. 8. (Color online) The relative displacement at which separation occurs (effective asperity length) vs cycle number from the molecular dynamics simulation. A linear trend line is drawn to guide the eye and illustrate the general trend toward asperity growth with increasing cycles.

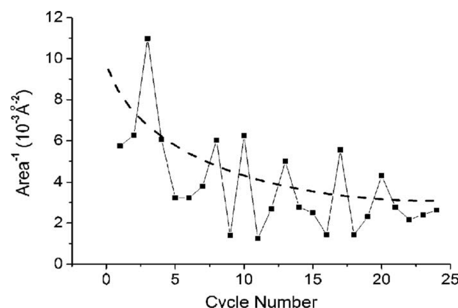

FIG. 10. (Color online) Initial contact area (proportional to contact resistance) when the surfaces are originally brought together as a function of cycle number. Initial contact area is defined to be the contact area upon application of a very small force (2 nN). A trend line is drawn simply to guide the eye.

substrate and the large (micron-sized) tip change as it roughens at the nanoscopic level. Large attractive forces, normally seen as tip and substrate are brought into close contact (e.g., approach 1 of Fig. 5), are systematically reduced as asperity growth continues. The distancing of the bulk tip from the substrate and the buildup of small repulsive forces associated with compressing the asperities serve to offset attractive van der Waals interactions.

Experimental and simulation results can be linked to the behavior of actual MEMS devices designed to operate at a fixed actuation voltage (applied force). In these devices, an initial decrease in resistance with cycling is observed.[3] It is common to attribute this decrease to the demolition of a contamination layer, and our studies show this is indeed a key factor but not the only one. Using the simulations, we can monitor the change in intimate (metal/metal) contact area, and thus effective resistance, without interference of contamination. As seen in Fig. 10, the resistance decreases as the system is cycled, showing that asperity evolution also contributes to the early lifetime behavior of the switch. The formation and growth of asperities (i.e., the texturing that is observed) is associated with the generation of defects. Until the defect density is sufficiently high (which leads to a hardening effect), defect incorporation results in a weakening of the material. A weakening effect is also seen in the compression of thin gold nanowires[35] where thinner wires are characterized by small compressive yield stresses. In this case, the weakening is attributed to surface stresses associated with atomistic surface rearrangements. Whether due to defect generation or surface rearrangements, the same applied force produces a larger area of intimate contact from one cycle to the next leading to a decrease in resistance.

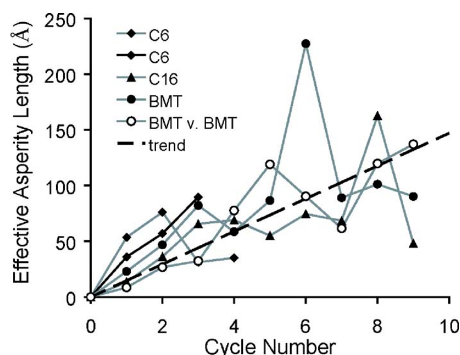

FIG. 9. (Color online) Trend of asperity growth (experimental data) with repeated cycling. General trend is toward growth, although the stochastic nature of the material transfer causes sometimes large fluctuations in length. A linear trend line is drawn to guide the eye.

In actual MEMS devices this resistance trend eventually reverses showing a gradual increase as switch cycling continues.[3] Transition to this late-life regime is controlled by the switch's inability to fully compress larger asperities with a set operating force. As cycles progress in the IFM experiments, we begin to see a change in the resistance response (Fig. 5, approach profiles 3 and 4) of these surfaces (i.e., the profiles get distinctly less sharp as cycling continues), an early indicator of transition to this late-life regime. As the nanoasperities gain mass and length, they eventually reach sufficient volume (with sufficient defect densities) such that work hardening effects come into play. In this regime, contact area will be limited to compression of only the longest asperities resulting in a decreased contact area (increased resistance) for a given applied load.[17]

One advantage of using a model switch is that it allows us to explore various parameters critical to the function of an operating switch, such as the amount of current passing through the contact. As might be expected, current also has an effect on the evolution and dynamics of the contact. Once intimate metallic contact is made, resistance drops and current begins to flow. Resistive heating in the contact zone causes an increase in temperature which fuses the contact spot when the melting point of the metal is realized[7] (nanospot welding). During retraction, this warm metallic bridge is extended and asperities form when the bridge eventually ruptures. We find that the amount of current passing through the weld affects the mechanism of rupture.

At high current, the presence of arcing is a distinctive representation of this weld's rupture mechanism. This is manifested in stochastic jumps in measured resistance, seen most notably in Fig. 2(b). As the weld is stretched, its decreasing cross-sectional area (increasing resistance) causes bridge temperature to rise. Ultimately, the bridge will boil releasing metallic vapor into the gap. In our measurement system, voltage increases as the bridge continuity breaks (re-

Downloaded 28 Jun 2007 to 128.112.35.157. Redistribution subject to AIP license or copyright, see http://jap.aip.org/jap/copyright.jsp

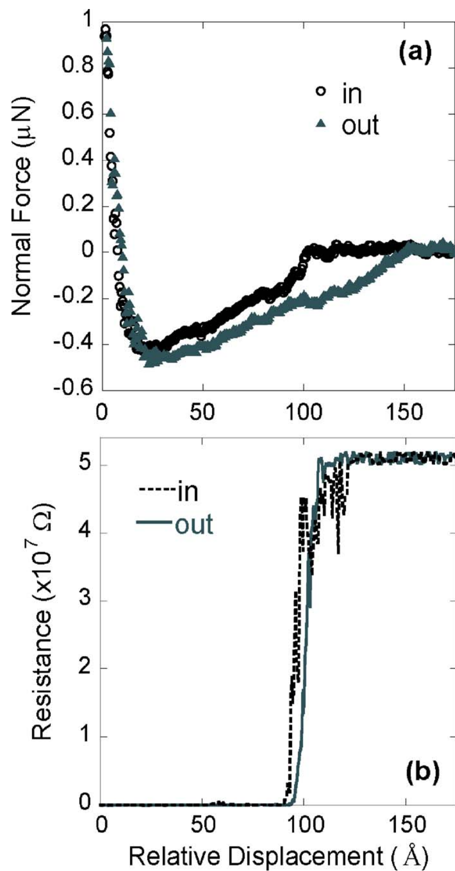

FIG. 11. (Color online) (a) Force and (b) electrical contact resistance profiles of a reapproach cycle using a lower current setting.

sistance going to infinity) creating a field sufficient to ionize the metallic vapor within the gap resulting in arcing.

Lower current density produces lower bridge temperatures delaying bridge boiling, which allows other instabilities (e.g., electromigration, convection due to temperature differences, meniscus deterioration, etc.) to dominate the rupture mechanism. Figure 11 demonstrates that if current is decreased, from 1 μA to 50 nA, we observe a consequential decrease in the amount of chaotic behavior, as well as a narrowing of the on/off transition. At the low current set point, the bridge ruptures before peak temperature is attained resulting in significantly less arcing and a more exacting switch performance.

IV. CONCLUSION

The interfacial force microscope (IFM) has been used to explore the fundamental processes involved in switch failure. As the primary focus of this investigation, the role of repetitive cycling on the evolution of surface topography and resistance in our model switch contact was examined. We find that cyclic contact degrades protective coatings (in the form of contamination or designer SAMs) eventually allowing localized penetration in the form of a "nanospot weld" between gold tip and substrate. The weld stretches as the tip is retracted, ultimately breaking, forming in a spikelike extremity. Fundamental processes such as asperity growth due to continued cycling result in an overall roughening of the surfaces that is corroborated in atomistic simulations. Changes in resistance, as a function of repeated cycling, are a consequence of these changes in surface topography and can be associated with trends seen in actual MEMS switches.

ACKNOWLEDGMENT

This work was supported by the National Science Foundation (MRSEC Program) through the Princeton Center for Complex Materials (DMR 0213706)

[1]E. R. Brown, IEEE Trans. Microwave Theory Tech. **46**, 1868 (1998), .
[2]G. M. Rebeiz, *RF MEMS: Theory, Design, and Technology* (Wiley-Interscientific, Hoboken, NJ, 2003).
[3]S. Majumder, N. E. McGruer, G. G. Adams, P. M. Zavracky, R. H. Morrison, and J. Krim, Sens. Actuators, A **A93**, 19 (2001).
[4]H. Lee, R. A. Coutu, S. Mall, and K. D. Leddy, J. Micromech. Microeng. **16**, 557 (2006).
[5]D. J. Wold and C. D. Frisbie, J. Am. Chem. Soc. **123**, 5549 (2001).
[6]J. W. Tringe, T. A. Uhlman, A. C. Oliver, and J. E. Houston, J. Appl. Phys. **93**, 4661 (2003).
[7]R. Holm, *Electric Contacts: Theory and Application*, 4th ed. (Springer-Verlag, New York, 1967).
[8]P. G. Slade, *Electrical Contacts: Principles and Applications* (Marcel Dekker, New York, 1999).
[9]A. Lumbantobing, L. Kogut, and K. Komvopoulos, J. Microelectromech. Syst. **13**, 977 (2004).
[10]B. L.Pruit and T. W. Kenny, Sens. Actuators, A **104**, 68 (2003).
[11]S. T. Patton and J. S. Zabinski, Tribol. Lett. **18**, 215 (2005).
[12]D. Hyman and M. Mehregany, IEEE Trans. Compon. Packag. Technol. **22**, 357 (1999).
[13]J. Beale and R. F. Pease, IEEE Trans. Compon., Packag. Manuf. Technol., Part A **17**, 257 (1994).
[14]J. Schimkat, Sens. Actuators, A **73**, 138 (1999).
[15]C. N. Neufeld and W. F. Rieder, IEEE Trans. Compon., Packag. Manuf. Technol., Part A **18**, 369 (1995).
[16]E. J. J. Kruglick and K. S. J. Pister, J. Microelectromech. Syst. **8**, 264 (1999).
[17]L. Kogut and K. Komvopoulos, J. Appl. Phys. **94**, 3153 (2003).
[18]K. Komvopoulos and N. Ye, Trans. ASME, J. Tribol. **123**, 632 (2001).
[19]J. Greenwood and J. Williams, Proc. R. Soc. London, Ser. A **295**, 300 (1966).
[20]W. R. Chang, I. Etsion, and D. B. Bogy, Trans. ASME, J. Tribol. **109**, 257 (1987).
[21]J. D. Kiely and J. E. Houston, Phys. Rev. B **57**, 12588 (1998).
[22]J. D. Kiely, R. Q. Hwang, and J. E. Houston, Phys. Rev. Lett. **81**, 4424 (1998).
[23]X. D. Xiao, G. Y. Liu, D. H. Charych, and M. Salmeron, Langmuir **11**, 1600 (1995).
[24]S. Xu and G. Y. Liu, Langmuir **13**, 127 (1997).
[25]R. D. Piner, J. Zhu, F. Xu, S. H. Hong, and C. A. Mirkin, Science **283**, 661 (1999).
[26]N. A. Amro, S. Xu, and G. Y. Liu, Langmuir **16**, 3006 (2000).
[27]J. Houston, in *Applied Scanning Probe Methods I*, edited by B. Bhushan and H. Fuchs (Springer-Verlag, Berlin, Heidelberg, 2004).
[28]J. E. Houston, C. M. Doelling, T. K. Vanderlick, Y. Hu, G. Scoles, I. Wenzl, and T. R. Lee, Langmuir **21**, 3926 (2005).
[29]M. S. Daw and M. I. Baskes, Phys. Rev. B **29**, 6443 (1984).
[30]S. M. Foiles, M. I. Baskes, and M. S. Daw, Phys. Rev. B **33**, 7983 (1986).
[31]J. Cai and Y. Y. Ye, Phys. Rev. B **54**, 8398 (1996).
[32]P. R. Cha, D. J. Srolovitz, and T. K. Vanderlick, Acta Mater. **52**, 3983 (2004).
[33]W. F. Rieder, IEEE Trans. Compon. Packag. Technol. **23**, 286 (2000).
[34]U. Landman, W. D. Luedtke, N. A. Burnham, and R. J. Colton, Science **248**, 454 (1990).
[35]J. K. Diao, K. Gall, M. L. Dunn, and J. A. Zimmerman, Acta Mater. **54**, 643 (2006).

Downloaded 28 Jun 2007 to 128.112.35.157. Redistribution subject to AIP license or copyright, see http://jap.aip.org/jap/copyright.jsp